LASER INDUCED GRATINGS IN Eu^{3+}- GLASSES

By

EDWARD GRADY BEHRENS

Bachelor of Science

Southeastern Oklahoma State University

Durant, Oklahoma

1984

Submitted to the Faculty of the Graduate College
of the Oklahoma State University
in partial fulfillment of the requirements
for the Degree of
MASTER OF SCIENCE
December, 1986

LASER INDUCED GRATINGS IN Eu^{3+} - GLASSES

Thesis Approved:

Richard C. Powell
Thesis Adviser

Larry E. Halliburton

George S. Dixon

Norman N. Durham
Dean of the Graduate College

ACKNOWLEDGMENTS

I would like to express my gratitude to all the people responsible for helping me during my studies at Oklahoma State University. Foremost among these is my thesis adviser, Dr. Richard C. Powell, who gave me the opportunity to begin research early in my graduate studies. I would also like to thank the other members of my committee, Dr. George S. Dixon and Dr. Larry E. Halliburton. I also wish to express my appreciation to Dr. Frederick M. Durville who assisted me in this work. Further, I wish to thank Mrs. Dee Behrens for her excellent typing of this manuscript.

Finally, I would like to thank the two people who have given me the inspiration to continue with my work, my wife, Linda and daughter, Crystal. Without their encouragement the long hours of work would not have been endurable.

Financial support for this work was provided by the U. S. Army Research Office and by the National Science Foundation under Grant No. DMR-82-16551.

TABLE OF CONTENTS

LIST OF TABLES

LIST OF FIGURES

CHAPTER I

INTRODUCTION

Statement of Problem

In recent years a lot of work has been devoted to the development of new optical devices designed to perform functions such as switching, modulation, phase conjugation, and bi-stability which are important in optical data processing. Glasses are attractive materials for these devices due to their affordability and ease of fabrication as opposed to single crystals. Laser-induced refractive index changes have been observed in several types of glasses (1-5) and used to produce holographic storage, narrow band filters, optical switching, and phase conjugation. However, in most cases, the physical mechanism responsible for producing the photorefractive change has not been explained. This thesis reports the observation of laser-induced superimposed transient and permanent refractive index changes in rare-earth doped glasses.

Summary of Thesis

In Chapter II the scattering efficiency of a monochromatic light wave off a grating is derived using a coupled wave approach. Chapter III describes the samples studied in this work. The experimental procedure is discussed along with the results. Chapter IV is a discussion of the effects observed. A physical mechanism is proposed to account for these observations.

CHAPTER II

THEORY

An important parameter measured in Four-Wave-Mixing (FWM) is the scattering efficiency, η, which can be derived theoretically using a coupled wave theory (6). A monochromatic light wave, R, with polarization perpendicular to the plane of incidence, is incident on the grating of thickness d. When the Bragg condition is met, a diffracted beam, S, is produced. This is shown graphically in Figure 1. The total electric field inside the grating is given as a superposition of the two waves

$$\vec{E} = R(z)\exp-(i\vec{k}_R\vec{x}) + S(z)\exp-(i\vec{k}_S\vec{x}) \tag{2-1}$$

where R(z) and S(z) are the amplitudes of the incident and diffracted beams, respectively. $\vec{k}_R$ and $\vec{k}_S$ are the wave vectors of the two waves which satisfy the Bragg condition

$$\vec{k}_g = \vec{k}_R - \vec{k}_S = k_g\hat{x} \tag{2-2}$$

where $\vec{k}_g$ is the grating wavevector with magnitude

$$|k_g| = 2\pi/\Lambda \tag{2-3}$$

and Λ is the grating period. For a wave propagating in the grating the electric field obeys the Helmholtz equation

$$\nabla^2\vec{E} + k^2\vec{E} = 0 \tag{2-4}$$

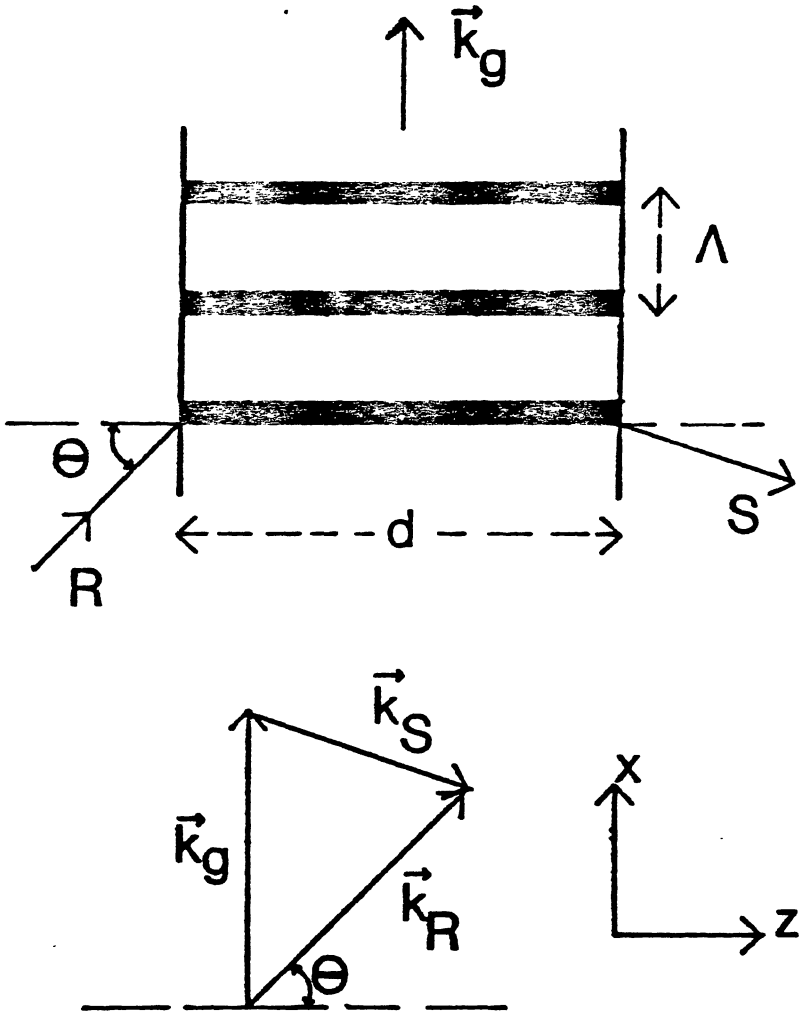

Figure 1. Coupled-Wave Model of Thick Gratings

where $\vec{E}(x,z)$ is the complex amplitude of the y-component of the electric field which is oscillating at a frequency ω. k^2, the propagation constant, is

$$k^2 = (\omega^2/c^2)\varepsilon + i\omega\mu\sigma \tag{2-5}$$

where c is the speed of light. ε and σ are the relative dielectric constant and conductivity, respectively, and μ is the permeability in free space.

The holographic grating can be expressed as a spatial modulation of ε and σ by

$$\varepsilon = \bar{\varepsilon} + \varepsilon_1 \cos(k_g x) \tag{2-6}$$

$$\sigma = \bar{\sigma} + \sigma_1 \cos(k_g x) \tag{2-7}$$

where $\bar{\varepsilon}$ and $\bar{\sigma}$ are the average dielectric constant and conductivity, ε_1 and σ_1 are the amplitudes of the spatial modulation. Insertion of equations (2-6) and (2-7) into equation (2-5) result in the following expression for the propagation constant

$$k^2 = (4\pi^2/\lambda^2)\bar{\varepsilon} + i(2\pi/\lambda)c\mu\bar{\sigma} + [(4\pi^2/\lambda^2)\varepsilon_1 + i(2\pi/\lambda)c\mu\sigma_1]\cos k_g x \tag{2-8}$$

where use has been made of the formula $\omega^2 = 4\pi^2 c^2/\lambda^2$. This simplifies to

$$k^2 = \beta^2 + 2i\alpha\beta + 4K\beta\cos k_g x \tag{2-9}$$

where the average propagation constant β and the absorption constant α have been introduced and are given by

$$\beta = (2\pi/\lambda)\bar{\varepsilon}^{\frac{1}{2}} \tag{2-10}$$

$$\alpha = c\mu\bar{\sigma}/2\bar{\varepsilon}^{\frac{1}{2}} \tag{2-11}$$

and the coupling constant, K, is

$$K = (\pi\varepsilon_1/2\lambda\bar{\varepsilon}^{\frac{1}{2}}) + i(c\mu\sigma_1/4\bar{\varepsilon}^{\frac{1}{2}}) \quad . \tag{2-12}$$

The coupling constant gives the coupling between R, the incident beam, and S, the diffracted beam. K is the central parameter in the coupled wave theory.

Optical media are usually described in terms of their refractive index and absorption coefficient. The complex index of refraction can be written as

$$\tilde{n} = n_R + in_I = n + i\lambda\alpha/4\pi \tag{2-13}$$

where n is the real index of refraction and α is the absorption coefficient. For a grating in which the index of refraction is spatially modulated, the amplitude of this modulation is given by Δn and $\Delta\alpha$

$$\Delta n \tilde{=} \varepsilon_1/2\bar{\varepsilon}^{\frac{1}{2}} \tag{2-14}$$

$$\Delta\alpha \tilde{=} c\mu\sigma_1/2\bar{\varepsilon}^{\frac{1}{2}} \quad . \tag{2-15}$$

Applying these to our coupling constant results in

$$K = (\pi/\lambda)\Delta n + i(1/2)\Delta\alpha \tag{2-16}$$

where we have assumed

$$\bar{\alpha},\ \Delta\alpha << (2\pi/\lambda)\bar{n} \text{ and } \Delta n << \bar{n}$$

$\bar{\alpha}$ and $\bar{n}$ are the average absorption constant and average index of refraction. The spatial modulation inferred by Δn and $\Delta\alpha$ couple the two waves R and S and leads to an exchange of energy. If K=0 there is no coupling and thus no diffracted wave. Equation (2-4) can now be written as

$$\nabla^2\vec{E} + (\beta^2 + 2i\beta\alpha + K\beta\cos k_g x)\vec{E} = 0 \ . \tag{2-17}$$

Inserting Equations (2-1) and (2-2) into Equation (2-17) leads to the following coupled equations

$$c_R R' + \bar{\alpha}R = iKS \tag{2-18}$$

$$c_S S' + \bar{\alpha}S = iKR \tag{2-19}$$

where $c_R = c_S = \cos\theta$. Higher order diffraction terms and second derivatives have been neglected. Bragg incidence and slow energy exchange and absorption have been assumed. The physical process involved in the diffraction can be seen in these equations. A wave incident on the grating changes amplitude along z due to the coupling of the other wave (KS,KR) or absorption ($\bar{\alpha}$S,$\bar{\alpha}$R).

The general solution to the above coupled equations is of the form

$$R(z) = r_1\exp(\gamma_1 z) + r_2\exp(\gamma_2 z) \tag{2-20}$$

$$S(z) = s_1\exp(\gamma_1 z) + s_2\exp(\gamma_2 z) \tag{2-21}$$

where r and s are constants which depend on the boundary conditions and γ_1 and γ_2 can be calculated by substituting Equations (2-20) and (2-21) into Equations (2-18) and (2-19)

$$\gamma_{1,2} = -\bar{\alpha}/\cos\theta \pm iK/\cos\theta \ . \tag{2-22}$$

For a transmission hologram we have the boundary conditons

$$R(0) = 1 \qquad S(0) = 0 \quad . \tag{2-23}$$

Inserting these into Equation (2-20) and (2-21) it is immediately seen

$$r_1 + r_2 = 1 \tag{2-24}$$

$$s_1 + s_2 = 0 \tag{2-25}$$

it is also seen that

$$s_1 = -s_2 = iK/c_s(\gamma_1 - \gamma_2) \quad . \tag{2-26}$$

Combining Equations (2-22) through (2-26) with Equation (2-21) generates

$$S(d) = [\exp-(\bar{\alpha}d/\cos\theta)] \quad [\exp(iKd/\cos\theta) - \exp-(iKd/\cos\theta)] \tag{2-27}$$

for the amplitude of the signal beam as a function of the grating thickness d.

The scattering efficiency η, is a measure of the amount of incident wave diffracted into signal wave and is defined as

$$\eta = SS^*$$

where the incident wave has been normalized. After some algebra the scattering efficiency reduces to

$$\eta = [\exp-(2\bar{\alpha}\zeta)][\sinh^2(\zeta/2)\Delta\alpha + \sin^2(\pi\zeta/\lambda)\Delta n] \tag{2-28}$$

with $\zeta = d/\cos\theta$. For normal incidence (θ=0) the scattering efficiency becomes

$$\eta = [\exp-(2\bar{\alpha}d)][\sinh^2(d/2)\Delta\alpha + \sin^2(\pi d/\lambda)\Delta n] \quad . \tag{2-29}$$

For a very small product of grating thickness and grating modulation

$$\eta = [\exp-(2\bar{\alpha}d)][(d/2)^2\Delta\alpha^2 + (\pi d/\lambda)^2\Delta n^2] \quad . \tag{2-30}$$

If there is no beam depletion as the wave traverses the crystal, which is a good assumption unless the wave is close to an absorption band, then η becomes

$$\eta = (1/2)^2[d^2\Delta\alpha^2] + (\pi/\lambda)^2[d^2\Delta n^2] \quad . \tag{2-31}$$

The scattering efficiency is usually determined experimentally. The quantities $\Delta\alpha$ and Δn are of importance as they give information on the type of grating formed.

One model used to evaluate $\Delta\alpha$ and Δn is given by Fayer and his group (7) and is outlined below. If the system is described by a damped harmonic oscillator model with the dispersion given by

$$\tilde{n}^2 - 1 = \sum_j N_j f_j'/(\omega_j^2 - \omega^2 - i\gamma_j\omega) = \sum_j n_j' \tag{2-32}$$

where N_j is the number density of the molecules in the initial state of the jth transition, ω_j and γ_j are the maximum oscillator frequency and the linewidth, respectively, and f_j' is the absorption strength, then the optical properties of the system can be related to excited state populations.

The real and imaginary parts of Equation (2-32) are

$$n_R^2 - 1 = \sum_j N_j f_j' (\omega_j^2 - \omega^2)/[(\omega_j^2 - \omega^2)^2 + \gamma_j^2\omega^2] = \sum_j n_{R_j}' \tag{2-33}$$

$$2n_R n_I = \sum_j N_j f'_j \gamma_j \omega / [(\omega_j^2 - \omega^2)^2 + \gamma_j^2 \omega^2] = \sum_j n'_{I_j} \tag{2-34}$$

where it has been assumed $n_I \ll 1$. The quantities n'_{R_j} and n'_{I_j} represent the contributions of the jth absorption band to n_R and n_I. If x is any parameter on which the optical properties are dependent, i.e. excited state concentration, then

$$dn_R/dx = (1/2n_o)(d/dx) \sum_j N_j f'_j (\omega_j^2 - \omega^2)/[(\omega_j^2 - \omega^2)^2 + \gamma_j^2 \omega^2] \tag{2-35}$$

$$dn_I/dx = (1/2n_o)(d/dx) \left\{ \sum_j N_j f'_j \gamma_j \omega / [(\omega_j^2 - \omega^2)^2 + \gamma_j^2 \omega^2] \right\} - (1/n_o)(dn_R/dx) n_I \tag{2-36}$$

where n_o is the unperturbed value of the refractive index. It grately simplifies matters to assume excitation wavelength close to the absorption wavelength, i.e. $\omega \simeq \omega_o$, and that there are no contributions from other absorption bands. Under these assumptions Equations (2-35) and (2-36) reduce to

$$dn_R/dx = (1/2n_o)(d/dx)\, 2N_o f'_o\, (\omega_o - \omega)/\omega_o [4(\omega_o - \omega)^2 + \gamma_o^2] \tag{2-37}$$

$$dn_I/dx = (1/2n_o)(d/dx) \gamma_o N_o f'_o / \omega_o [4(\omega_o - \omega)^2 + \gamma_o^2] \tag{2-38}$$

where the assumption $\omega_o^2 - \omega^2 = (\omega_o + \omega)(\omega_o - \omega) \simeq 2\omega_o(\omega_o - \omega)$ has been used. A term depending on (dn_R/dx) and k has been neglected since both are much less than unity.

If the ground state population density is given by N_o and the excited state peak population by N_{2P} then the phase grating modulation becomes

$$\Delta n = (dn_R/dN_o)\Delta N_o = -N_{2P}(f_o'/n_o)(1 - \omega/\omega_o)/[4(\omega_o - \omega)^2 + \gamma_o^2] . \quad (2\text{-}39)$$

The time dependence of the excited state population density can be written as

$$N_{2P}(t) = N_{2P}(0)\exp-(K/2)t \quad (2\text{-}40)$$

from which Equation (2-39) becomes

$$\Delta n(t) = -N_{2P}(0)\exp-(K/2)t\,[f_o'/n_o](1 - \omega/\omega_o)/[4(\omega_o - \omega)^2 + \gamma_o^2] \quad (2\text{-}41)$$

where K is the fluorescent decay rate. The intensity dependence is given by

$$N_{2P}(I) = N_o\sigma_1 I/[(h\nu/\tau) + \sigma_1 I] \quad (2\text{-}42)$$

where σ_1 is the ground state absorption cross section and τ is the fluorescent lifetime. This leads to

$$n(I) = -\frac{N_o\sigma_1 I(f_o'/n_o)(1 - \omega/\omega_o)}{[(h\nu/\tau) + \sigma_1 I][4(\omega_o - \omega)^2 + \gamma_o^2]} \quad (2\text{-}43)$$

The amplitude grating modulation $\Delta\alpha$, which is related to Δn_I by

$$\Delta n_I = (\lambda/4\pi)\Delta\alpha \quad (2\text{-}44)$$

is given by

$$\Delta\alpha = (4\pi/\lambda)\Delta n_I = (4\pi/\lambda)(dn_I/dN_o)\Delta N_o \tag{2-45}$$

$$\Delta\alpha = -(4\pi/\lambda)N_{2P}(1/2n_o)\ f_o'\gamma_o/\omega_o[4(\omega_o - \omega)^2 + \gamma_o^2] \tag{2-46}$$

and the same steps as previously followed will give the amplitude modulation as a function of time or intensity. Upon substituting Equations (2-39) and (2-46) into Equation (2-31) the scattering efficiency becomes

$$\eta = \frac{(\pi dN_{2P}f_o')^2[\gamma_o^2 + 16\omega_o^2(1 - \omega/\omega_o)^2]^2}{\left\{4\lambda n_o\omega_o[4(\omega_o - \omega)^2 + \gamma_o^2]\right\}^2} \tag{2-47}$$

Another method for calculating the amplitude grating modulation was given by Hill (8) for a simple two-level system. The absorption coefficient is given as

$$\alpha(\nu) = \sigma_1(\nu)N_o + [\sigma_2(\nu) - \sigma_1(\nu)]N_{2P} \tag{2-48}$$

where σ_1 and σ_2 are the ground and excited state absorption cross-sections and $N_o = N_1 + N_{2P}$ is the total concentration of active ions in the ground and excited states. For an excited state concentration given by

$$N_{2P} = N_o\sigma_1(\nu)I/[(h\nu/\tau) + \sigma_1 I] \tag{2-49}$$

the absorption coefficient becomes

$$\alpha(\nu) = N_o\sigma_1(\nu)\left\{1 + I[\sigma_2(\nu) - \sigma_1(\nu)]/[(h\nu/\tau) + \sigma_1(\nu)\ I]\right\}. \tag{2-50}$$

Assuming the intensity varies sinusoidally according to

$$I(\nu) = I_o[1 + \sin (2\pi/\Lambda)\hat{k}\cdot\vec{r}] \tag{2-51}$$

one can calculate the modulation of the absorption coefficient

$$\Delta\alpha = \alpha_P - \alpha_V = (\sigma_2 - \sigma_1)N_{2P} \ . \tag{2-52}$$

Using Equations (2-40) and (2-42) for the time and intensity dependence of N gives

$$\Delta\alpha(t) = (\sigma_2 - \sigma_1)N_{2P}(0) \exp - (K/2)t \tag{2-53}$$

and

$$\Delta\alpha(I) = (\sigma_2 - \sigma_1)N_o\sigma_1 I/[(h\nu/\tau) + \sigma_1 I] \ . \tag{2-54}$$

Δn is not treated in this two-level system.

CHAPTER III

EXPERIMENTAL RESULTS

Samples

Six samples were investigated in this study with only three responding to the FWM procedure. The samples are listed in Table I with the chemical composition of the host and the concentration of Eu^{3+} dopant listed in the mole percent. The three samples that produced a FWM signal were: EP, LP, and NS with sample sizes of 7.60 x 6.75 x 1.00 mm, 14.70 x 11.20 x 3.25 mm and 6.20 x 6.15 x 4.30 mm, respectively. General spectroscopic properties of the samples have been previously reported (9).

Procedures

The general FWM set-up used in this study is illustrated in Figure 2. For the individual experiments slight modifications were made. A Spectra-Physics Model 164 Argon-Ion Laser tuned to 4658 Å was used throughout the study. The path lengths of the two write beams were measured before each experiment to insure differences in the lengths were within the coherence length of the laser.

In order to measure the scattering efficiency of the samples a Spectra-Physics Stabilite Model 1205 Helium-Neon Laser of wavelength 6328 Å was shown through the sample. A Scientech Model 36-2002 Power and Energy Indicator was then inserted to measure the intensity of the beam after transversing the sample. The power meter was then removed and a

TABLE I

Eu^{3+}-DOPED GLASSES AND PROPERTIES

Sample	Network Formers	Network Modifiers	Eu^{3+} Content
EP	83.3 P_2O_5		16.7 Eu_2O_3
LP	52.3 P_2O_5	30.0 Li_2O 10.0 CaO 4.7 Al_2O_3	3.0 Eu_2O_3
NS	72.0 SiO_2	15.0 Na_2O 5.0 BaO 5.0 ZrO	3.0 Eu_2O_3
ZF	57.0 ZrF_4	34.0 BaF_2 4.0 AlF_3 3.0 LaF_3	2.0 Eu_2O_3
LB	59.0 B_2O_3	40.0 Li_2O	1.0 Eu_2O_3
KB	69.0 B_2O_3	30.0 K_2O	1.0 Eu_2O_3

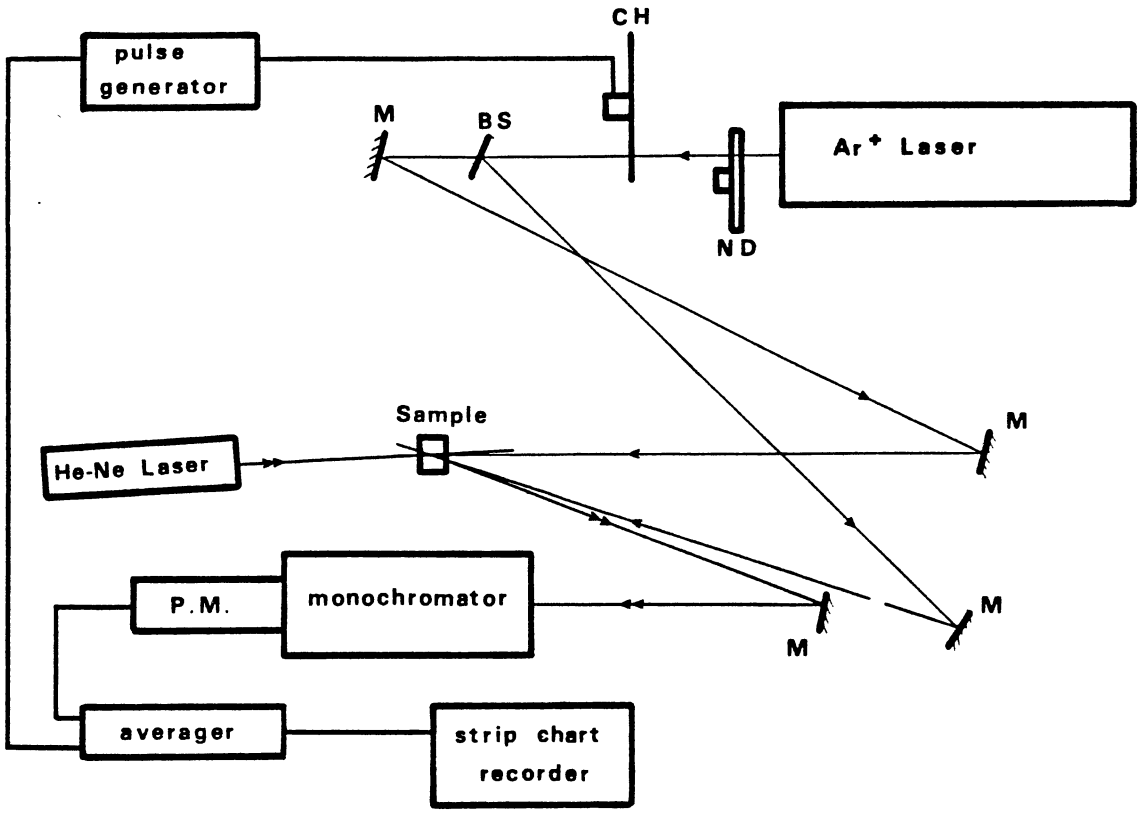

Figure 2. Schematic Diagram of the Experimental Setup Used in the Laser-Induced Grating Experiments. ND-Variable Neutral Density Filter; CH-Chopper; BS-Beam Splitter; M-Mirror

grating was established in the sample with the argon-ion laser. The He-Ne beam was then shown on the grating. The intensity of the diffracted signal beam was then recorded by the power meter. The ratio of these two measurements gives the experimental value of the scattering efficiency.

In taking lifetime measurement an HMS Lightbeam Chopper Model 220 was inserted prior to the splitting of the argon-ion laser beam. The beams were then aligned to form a grating in the sample. The He-Ne laser was used to probe the grating. The signal beam was passed through a .25m Pacific Instruments Model MP-1018B spectrometer to eliminate background due to fluorescence. A Hamamatsu Model R1547 photomultiplier tube was then used to collect the signal. The signal was processed by an EG&G Princeton Applied Research Corporation Model 4202 Signal Averager before being recorded by a Houston Omniscribe Series D5000 Recorder.

For the longtime data recorded, a grating was formed by the argon-ion beam and the He-Ne laser was used to probe this grating. The beams were not chopped. The signal was sent through the monochromator to the photomultiplier tube. The output of the photomultiplier was sent directly to the strip-chart recorder. The signal intensity could then be measured for time periods on the order of minutes to hours.

The low temperature data recorded on the EP sample was taken using the same procedures as outlined above except for the installation of the refrigerator. The EP sample was mounted inside a Cryosystems Model 22 Coldhead which was mounted on a CTI Cryogenics Model 22C Cryodyne Cryocooler. The data were taken at a temperature of 25 K.

In measuring the time dependence of the write beams, after forming a grating, the power meter and the photomultiplier tube were aligned to

pick up the write beams. The respective signals were then sent to two identical strip-chart recorders to compare the relative intensities.

Results

In the study the three samples that produced FWM signals: EP, LP, and NS, were subjected to numerous experiments. The same qualitative behavior was observed in all three samples. When the sample was illuminated by the write beams a small signal was observed immediately, followed by a gradual buildup of signal intensity. Figure 3 demonstrates the buildup of the signal intensity. The time to reach the maximum FWM signal intensity is on the order of minutes with the exact time depending on sample, laser power and wavelength. If the laser wavelength is not in resonance with a Eu^{3+} absorption transition, no signal is observed under these experimental conditions. This is consistent with the small values of the third order susceptibility tensor components measured by other techniques (10,11) and demonstrates the significant enhancement of the nonlinear optical properties of the material which can be realized by resonantly pumping a rare earth ion absorption transition. When the write beams are blocked the FWM signal intensity initially decreases, not back to the baseline but rather to a value of approximately seventy percent of the maximum FWM signal which will be referred to as the permanent signal. In the NS sample there is a slight resurgence in FWM signal intensity before levelling off to this constant value. If the write beams are left on over long periods of time the signal intensity fluctuates as shown in Figure 4 for the EP and NS samples. These fluctuations were seen for all samples regardless of write beam crossing angle. The

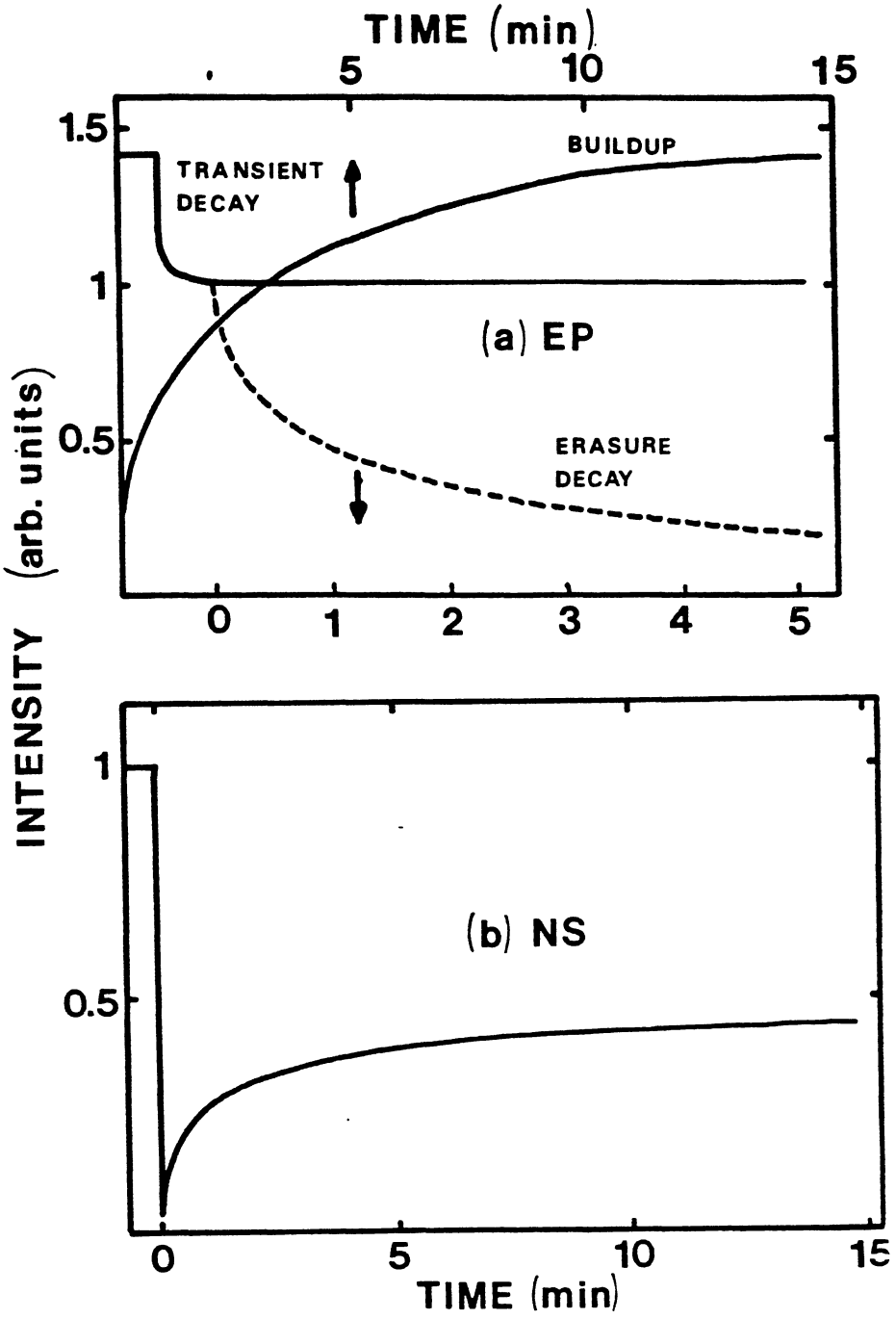

Figure 3. Time Evolution of the Buildup, Transient Decay, and Erasure of FWM Signals in EP (a) and NS (b) Glasses at 300 K. The Total Power of the Laser Write Beams is 80 mW and the Erase Beam Power is 40 mW

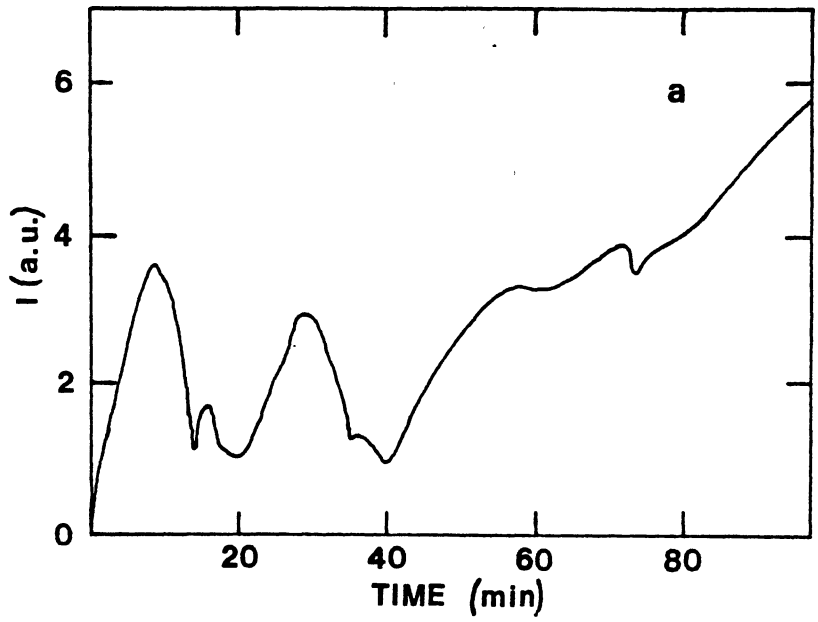

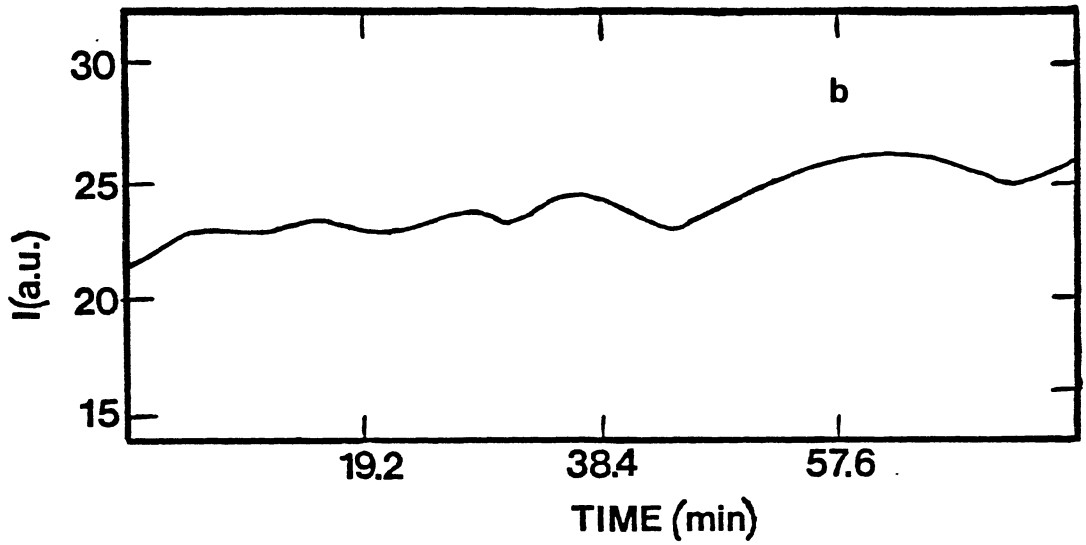

Figure 4. Evolution of FWM Signal in a) EP and b) LP

source of these fluctuation, whether mechanically introduced or as a result of the laser interaction with the sample, is still unknown.

When the write beams are chopped off, the initial FWM signal decays exponentially with a decay rate equal to .385 ms^{-1} as shown in Figure 5. This is the same as the fluorescence decay rate of .370 ms^{-1} measured for the $^5D_0$ metastable state transition of Eu^{3+} in these samples (9). The lack of transient grating lifetime dependence on write beam crossing angle, as shown in the previous figures, implies that there is no coupling between the two write beams (12). This is graphically demonstrated in Figure 6 for the EP sample.

The permanent signal remains at the same high level for days. It can be erased by focusing a single laser beam on the same region of the sample in resonance with a Eu^{3+} absorption transition. The erasure time is on the order of minutes with the exact time depending on temperature and laser power. From Figure 7 we see that the erasure rate of the permanent signal is constant for the EP and NS samples but is dependent on angle for the LP sample. As seen in Figure 3, the time dependence of the permanent signal erasure is highly nonexponential. However, a characteristic decay time equal to the e^{-1} value for the signal can be defined to describe the speed of the erasure under specific experimental conditions. Figure 8 shows the variation of the erasure decay rate versus temperature in the range 294 to 500 K depending on sample. The erasure decay rate increases exponentially as temperature is raised. This temperature dependence can be described by an expression of the form

$$K \alpha \exp[-\Delta E/kT] \qquad (3\text{-}1)$$

where ΔE is the activation energy for the process and k is Boltzmann's

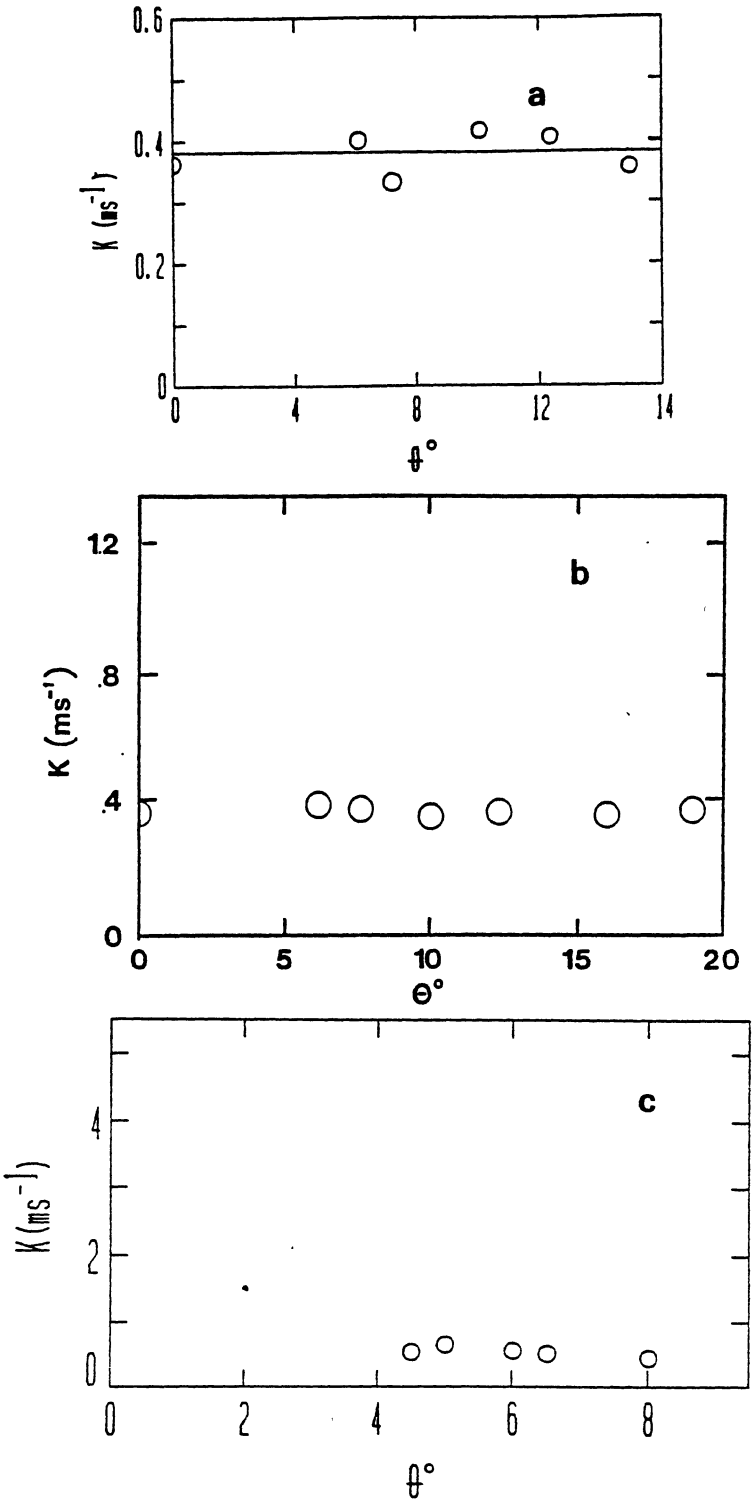

Figure 5. Decay Rate Versus Angle for Transient Grating in a) EP, b) LP, and c) NS

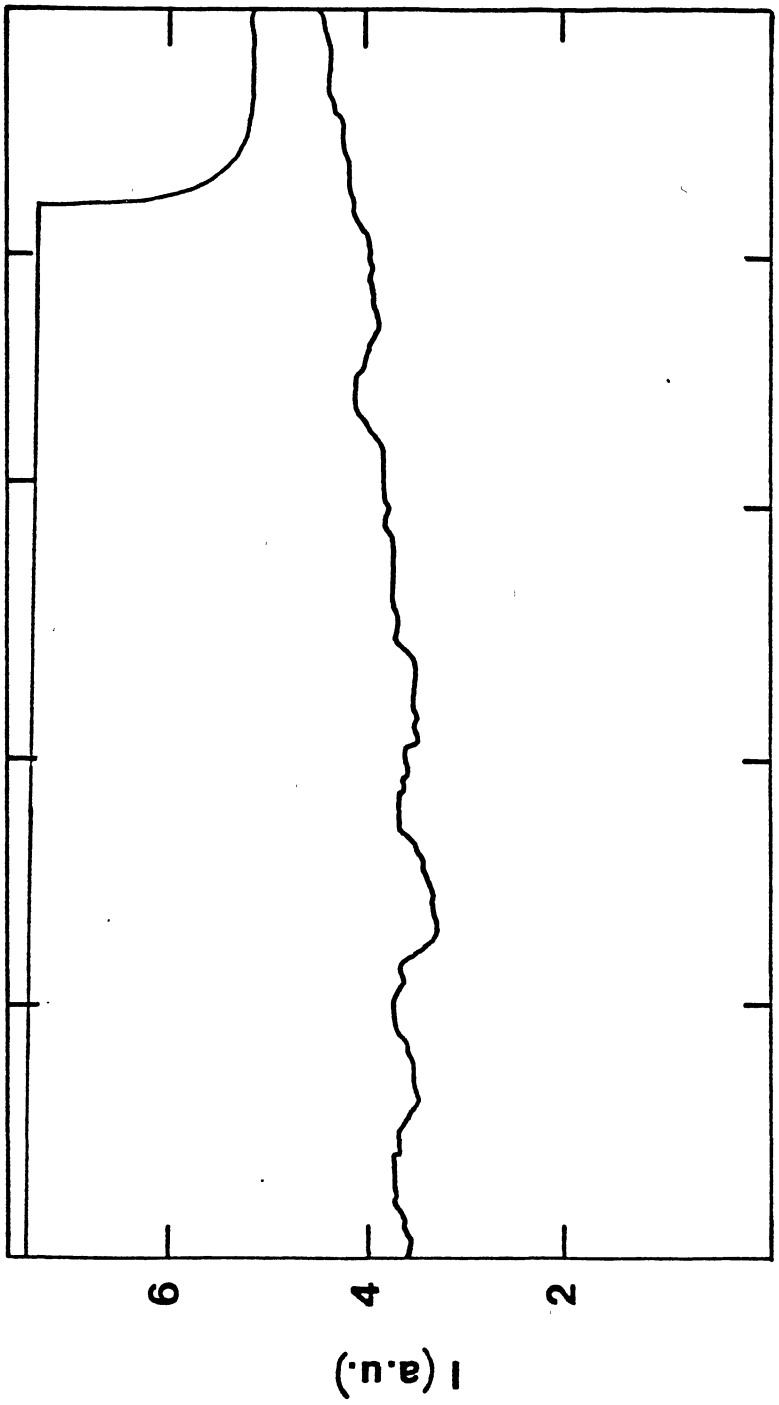

Figure 6. Evolution of Write Beam Intensities in EP

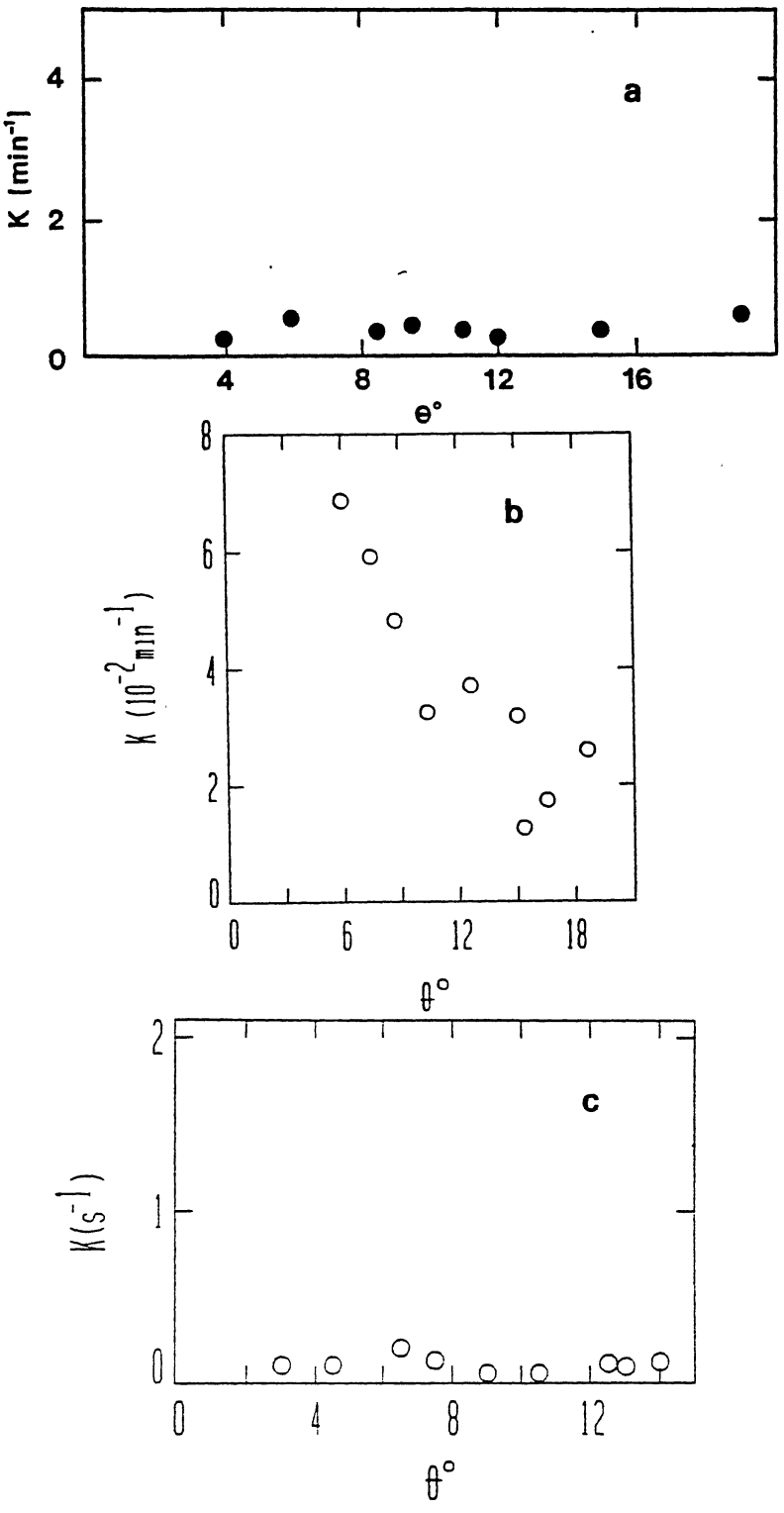

Figure 7. Erasure Rate Versus Angle for Permanent Grating in a) EP, b) LP, and c) NS

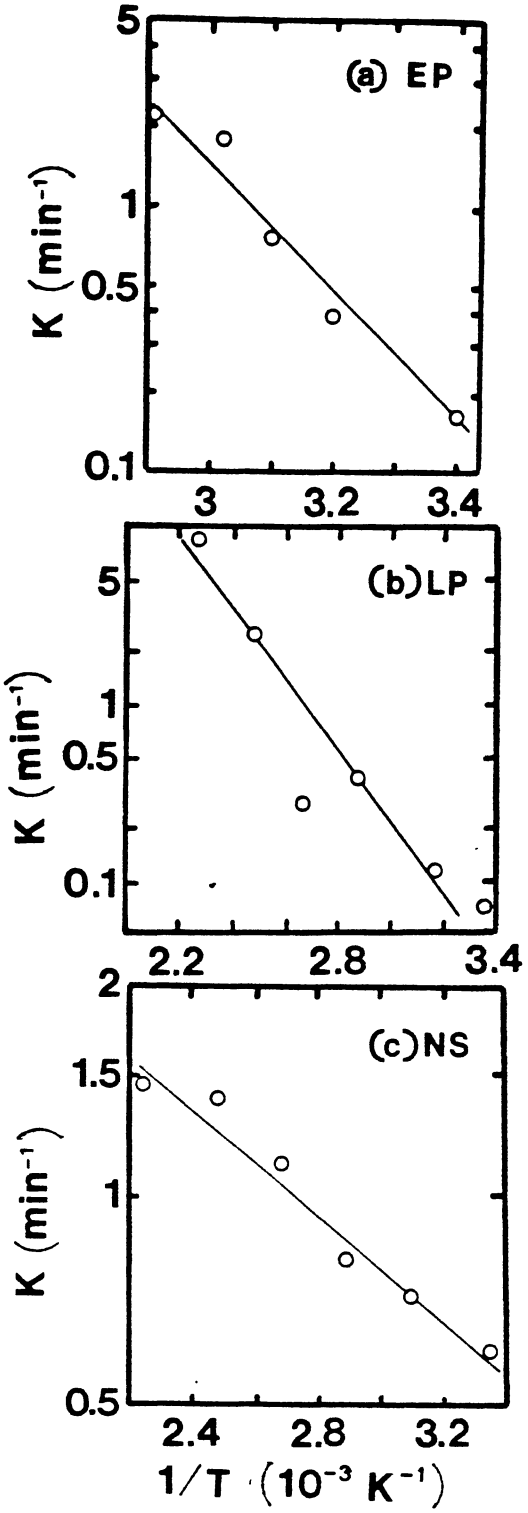

Figure 8. Erasure Decay Rate of the Permanent FWM Signal as a Function of Temperature for a) EP, b) LP, and c) NS at $\Theta=7^{o}$. The Laser Power in the Erase Beam is 40 mW

constant. The slope of the curves in Figure 8 gives an activation energy of 4016 cm^{-1} for EP, 3213 cm^{-1} for LP, and 614 cm^{-1} for NS. Figure 9, which gives the variation of the permanent and transient FWM signal intensities as a function of temperature of formation of the laser-induced grating gives values for ΔE of 2219 cm^{-1} for EP, 3824 cm^{-1} for LP, and 699 cm^{-1} for NS. Figures 10 and 11 show that the intensity of the FWM signal decreases as the temperature is raised above room temperature. The permanent grating can be erased by heating the samples to about 380 and 417 K for EP and LP, respectively. The temperature dependence of the scattering efficiency is consistent with a thermal activation energy of 3983 cm^{-1} for EP, 2101 cm^{-1} for LP, and 2890 cm^{-1} for NS which is not shown.

The signal intensity, expressed in terms of the scattering efficiency of the probe beam η, also varies with the crossing angle of the write beams as shown in Figure 12. For both permanent and transient signals the scattering efficiency is largest at small crossing angle. This is typical behavior for FWM signals with the exact form depending on the coupling mechanism for the beams (12).

Figure 13 displays the FWM signal intensity versus total write beam laser power. The transient term is linearly dependent on the power whereas the permanent term shows a quadratic dependence up to about 100 mW where saturation occurs.

Low temperature measurements were attempted and the transient decay rate was recorded for the EP sample at approximately 30 K. Figure 14 displays this measurement and shows there is no significant change from the room temperature data.

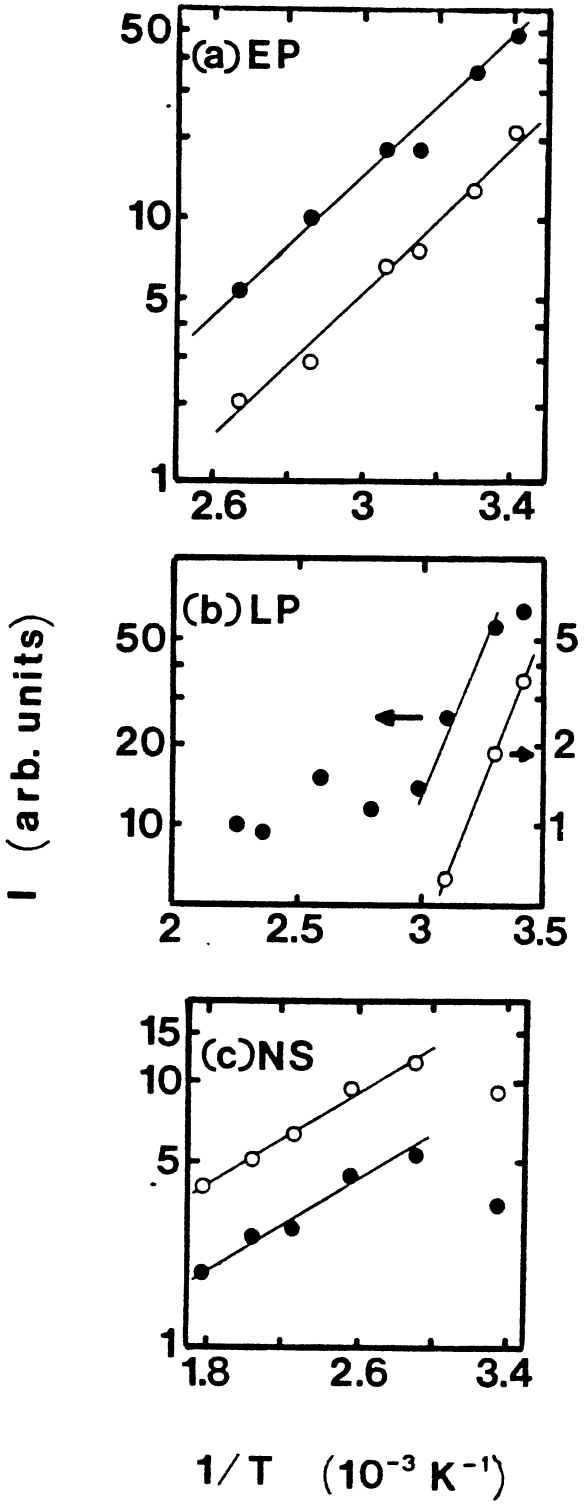

Figure 9. Variation of the Permanent (o) and Transient (o) FWM Signal Intensities as a Function of Temperature of Formation of the Laser-Induced Gratings for a) EP, b) LP, and c) NS Samples

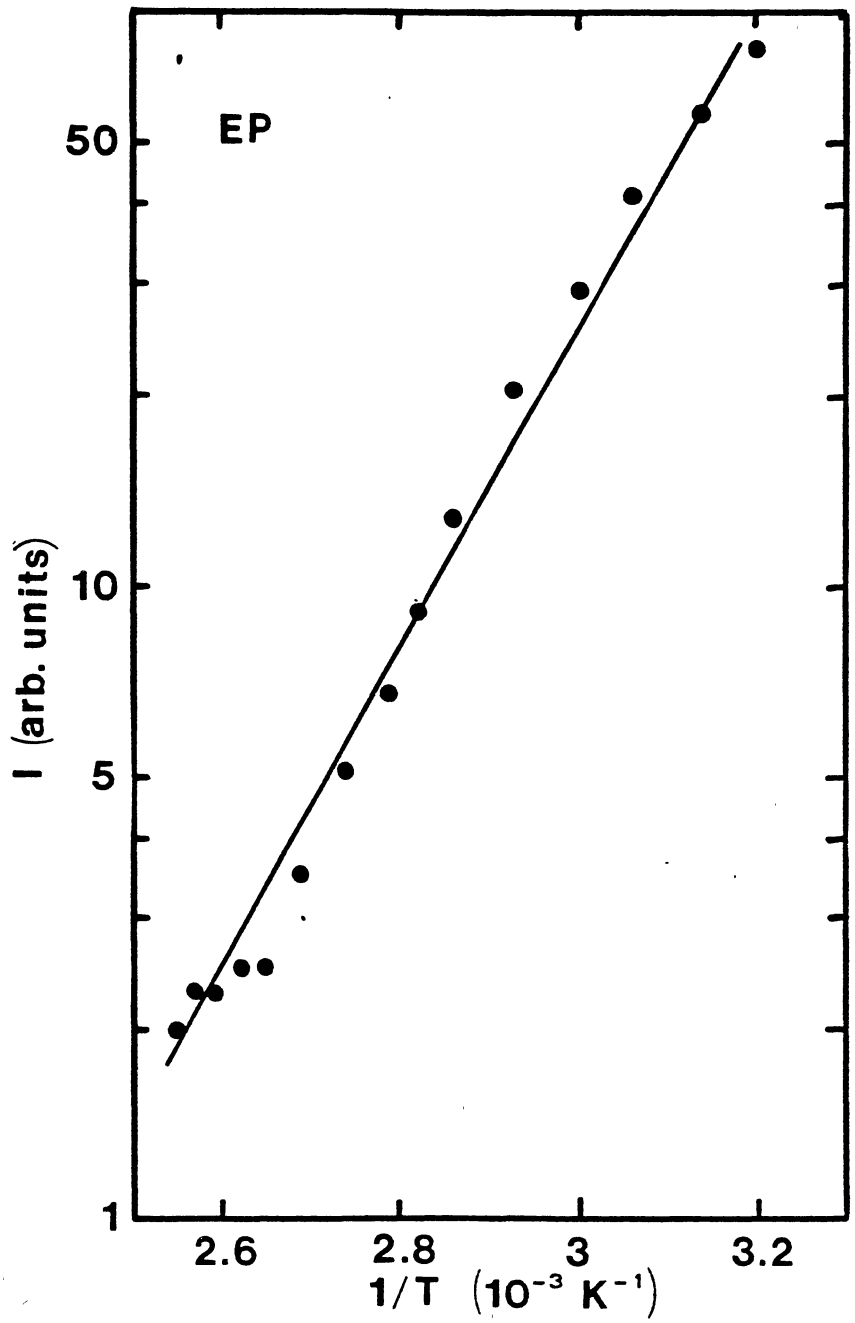

Figure 10. Variation of the Permanent FWM Signal Intensity as a Function of Temperature After Laser-Induced Grating Formation at 300 K in EP

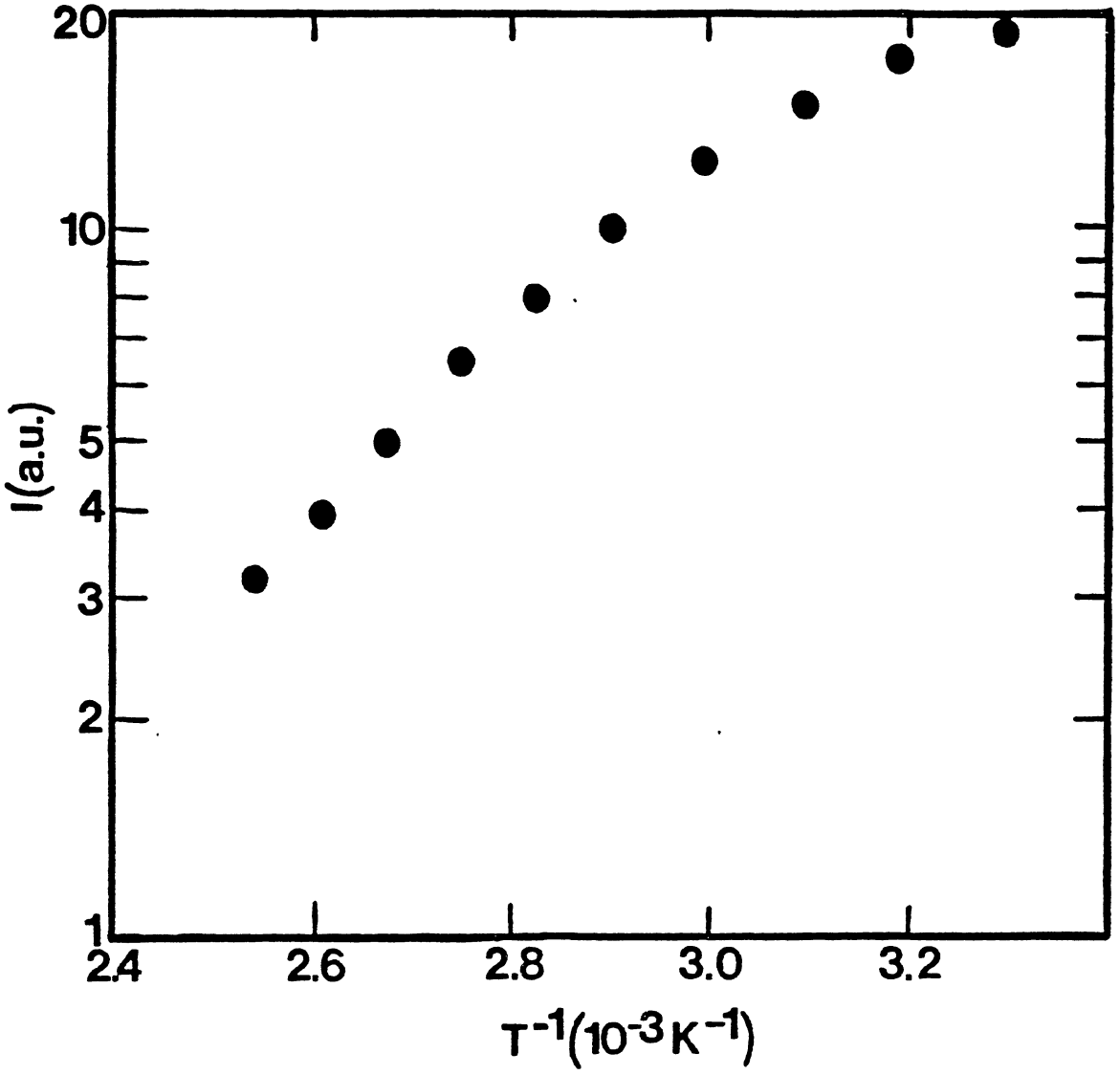

Figure 11. Variation of the Permanent FWM Signal Intensity as a Function of Temperature After Laser-Induced Grating Formation at 300 K in LP

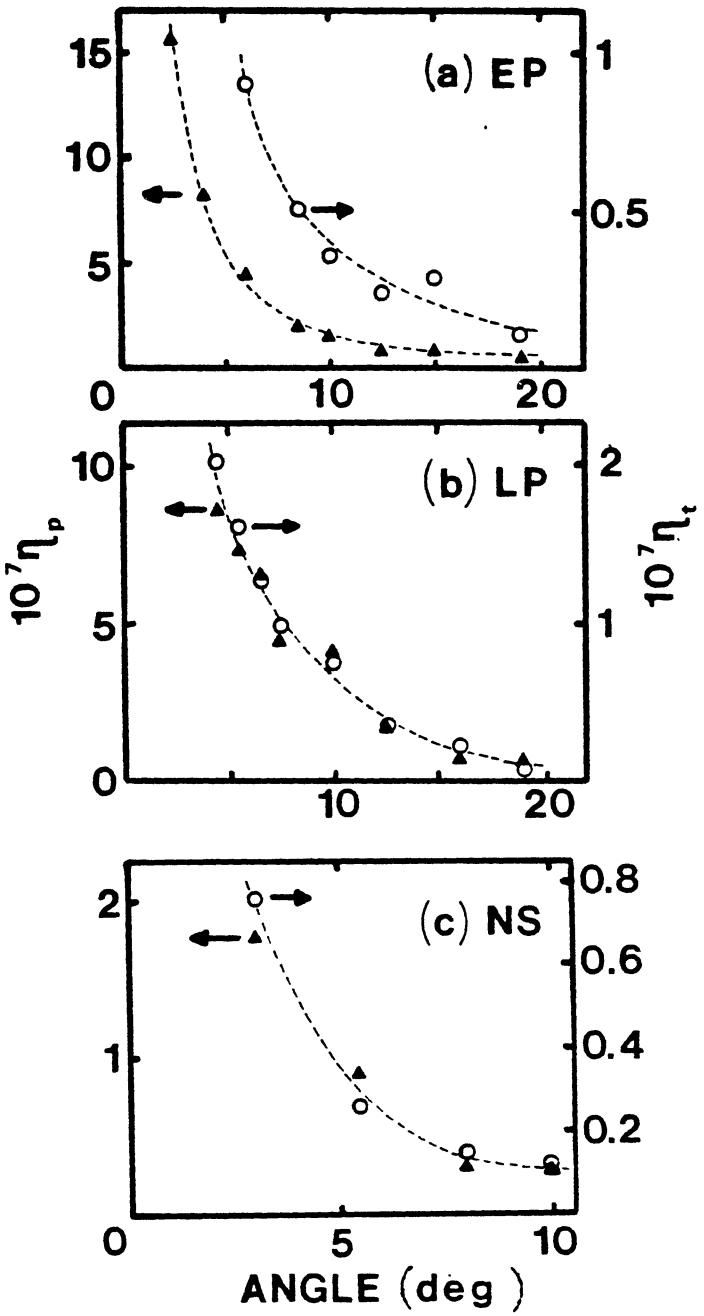

Figure 12. Transient (o) and Permanent (▲) FWM Signal Efficiencies as a Function of the Crossing Angle of the Write Beams in Air at 300 K. a) EP Glass; b) LP Glass; c) NS Glass

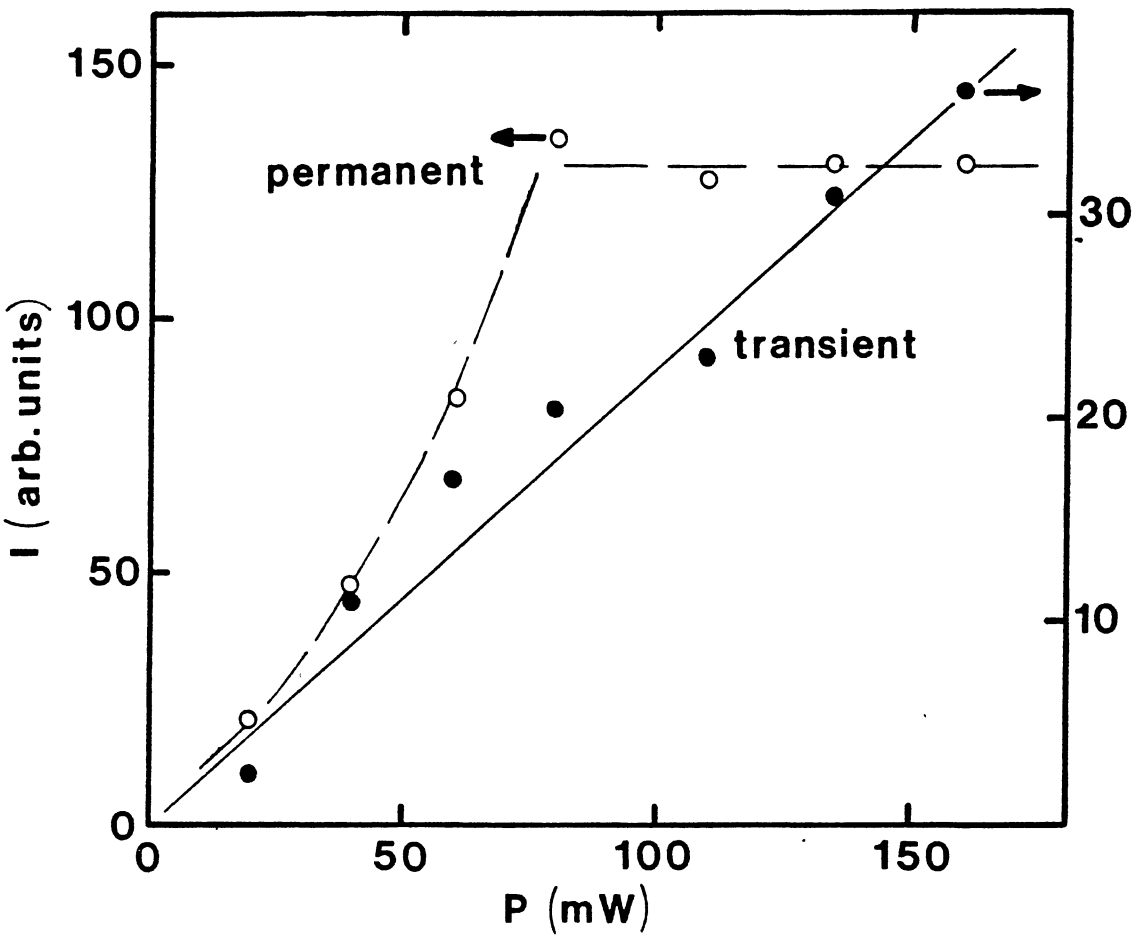

Figure 13. Transient and Permanent FWM Signal Intensities as a Function of Total Write Beam Laser Power for EP at 300 K

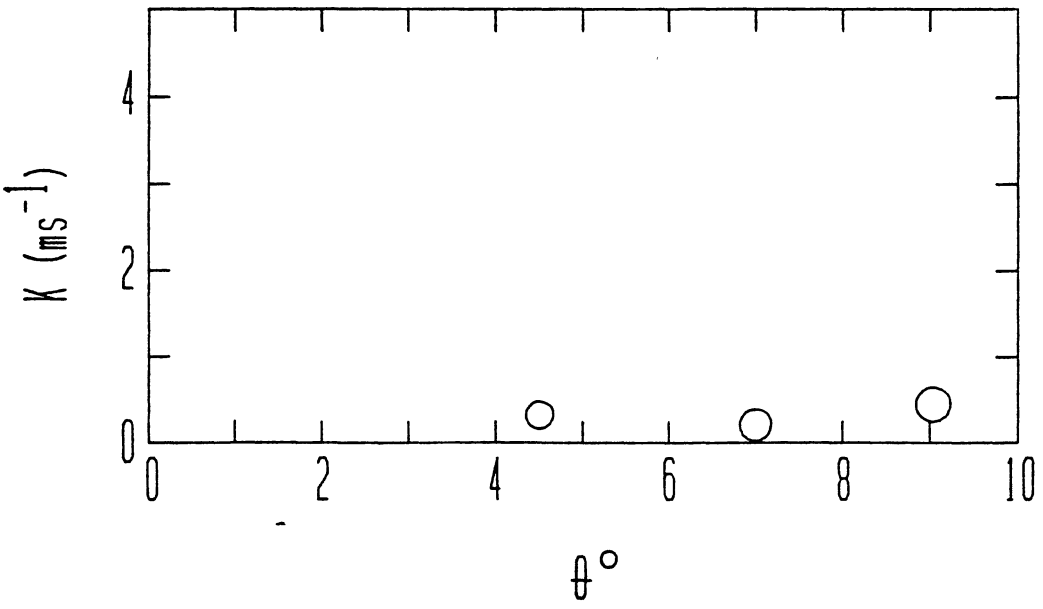

Figure 14. Decay Rate Versus Angle for Transient Grating at Low Temperature in EP

CHAPTER IV

DISCUSSION AND CONCLUSION

Interpretation of Results

The FWM signal observed here is significantly different than what has previously been seen (13-17). The characteristics of this signal are discussed below:

1. The signal is observed only when the laser write beams are crossed. No effect is seen when the sample is illuminated with only a single beam.

2. A grating is only formed when Eu^{3+} ions are resonantly excited.

3. The transient signal has a lifetime of about 2.7 ms independent of write beam crossing angle. This is precisely the fluorescent lifetime.

4. The permanent signal exhibits a risetime of the order of minutes and is power independent.

5. The intensities of the permanent signal and transient signal are temperature dependent.

6. Erasure of the permanent grating can be accomplished by illuminating the grating with the laser tuned to the Eu^{3+} resonance. The erasure rate is of the order of tens of minutes, independent of write beam crossing angle, and shows an exponential temperature dependence.

The results listed above and in Chapter III are consistent with the scattering of the FWM signal from two, super-imposed gratings. The

intensity of the FWM signal is proportional to the square of the laser-induced change in the refractive index produced in the sample by the crossed laser beams. The laser-induced change in the refractive index in this case is the sum due to the transient component of the grating, with lifetime τ_T, and that due to the permanent component of the grating, $\Delta n \propto \Delta n_T + \Delta n_P$. The FWM signal intensity is given by

$$I_S \propto |\Delta n_T|^2 e^{-2t/\tau} + 2|\Delta n_T|\,|\Delta n_P| e^{-t/\tau} + |\Delta n_P|^2 \quad . \qquad (4\text{-}1)$$

The first term is negligible compared to the last two as can be seen in Figure 2.

Transient Grating

Equation 4-1 predicts a transient grating with a decay time the same as the fluorescent decay time. This is consistent with number three in the characteristics listed above. Since the transient component decays with the fluorescent decay time of the ^5D_o metastable state and no grating is formed unless the Eu^{3+} ions are directly excited implies that the transient grating is associated with a population grating of Eu^{3+} ions in the ^5D_o metastable state. Since the crossing angle of the write beams determines the grating spacing and there was no Θ dependence of the decay rate, it can be assumed that there is no long range energy transfer in the excited state.

The second term in Equation 4-1 also predicts that the intensity of the transient component of the FWM signal is linearly dependent on the laser power. This is consistent with Figure 13. The measurements of the transient and permanent signal intensities took place after the permanent signal had reached its maximum. Thus the measured variation of the

transient grating scattering efficiency may be associated with the presence of the strong permanent grating.

The behavior of the scattering efficiency as the write beam angle is varied is typical of FWM signals (12). The temperature variation of the FWM signal intensity is the same for both the transient and permanent gratings. This implies that the laser-induced changes vary in the same way with temperature. The solid lines drawn in Figure 9 describe an exponential temperature variation

$$I = I_o e^{\Delta E_f'/kT} \qquad (4\text{-}2)$$

where $\Delta E_f'$ is the activation energy and k is Boltzmann's constant. The values obtained for $\Delta E_f'$ for each sample are listed in Table II and their physical meaning will be discussed below.

Permanent Grating

The scattering of the read beam from the permanent grating is described by the second and third terms in Equation 4-1. The second term describing the interference between the signals of the permanent and transient gratings. The fact that the permanent grating takes times of the order of tens of minutes to build up and then shows no decay over a period of days indicates that the interference pattern of the write beams has created a permanent structural change in the glass host. However, this change is only seen if the laser beams directly interact with a resonant transition of the Eu^{3+} ions and the write beams cross inside the sample.

Equation 4-1 predicts a quadratic dependence of the signal intensity from the permanent grating on the power of the laser write beams. This

TABLE II

SUMMARY OF RESULTS

Parameter	Sample		
	EP	LP	NS
τ_f(ms)	2.7	2.8	2.7
τ_t (ms)	2.67	2.85	2.86
τ_{rise}(min)	15	30	0**
ΔE_g(cm^{-1})	3983	2101	2890
ΔE_{eo}(cm^{-1})	4016	3213	614
$\Delta E_f'$(cm^{-1})	2219	3824	699

**After the write beams were turned off, a rise time of about 5 min. was observed.

is precisely what is observed and illustrated in Figure 13. The observed saturation shows that there is a limit to the structural modification of the glass. The decrease in scattering efficiency with increasing write beam crossing angle as seen in Figure 12 is typical of FWM signals, as mentioned above.

Figure 2 shows that the permanent signal can be erased, which implies that the laser-induced structural modification of the glass is reversible. The fact that the erasure decay rate is independent of write beam crossing angle implies that the glass modification does not involve long range migration of charge carriers. Since erasure can occur thermally and by directly exciting an Eu^{3+} absorption transition, the structural modification can be erased with the Eu^{3+} ions either in the ground or excited state.

The observed temperature dependences of the signal intensities and erasure rates are consistent with exponential processes having activation energies ΔE_g for thermal erasure and ΔE_{eo} for thermally assisted optical erasure. The solid lines in Figures 8, 9 and 10 represent the best fits to the experimental data with an exponential expression. The values for the activation energies are listed in Table II. The value of ΔE_g was obtained from the data in Figures 10 and 11 and represents the activation energy of thermal erasure with the Eu^{3+} ions in the ground state. The value of ΔE_{eo} was obtained from the data in Figure 8 and represents the activation energy of thermally assisted optical erasure with the Eu^{3+} ions in the excited state. The value of ΔE_f was obtained from the data in Figure 9 and represents the thermal activation energy associated with the grating formation process. This may be affected by the concurrent erasure

during grating formation, by thermal population of higher Eu^{3+} levels, or by thermally activated energy migration.

Mechanism

As stated above the transient signal is associated with a laser-induced population grating of the Eu^{3+} ions. Population gratings are well understood and have been investigated previously (4,13). Thus, the subject of this chapter is to discuss the mechanism responsible for the creation of the permanent grating.

The FWM signal observed here is not associated with an isolated population grating, but with the interference between a permanent grating and a transient grating. According to Equation 4-1, the intensity variations of the signal associated with this interference term will depend on the variation of the permanent grating. Whereas the decay rate will be described by the fluorescent decay rate. This accurately describes the observations for each of the three samples.

Permanent gratings can be created by crossed laser beams through several physical mechanisms. The most common mechanism is the photorefractive effect associated with the photoionization of defects and subsequent trapping of the free carriers (18). This type of mechanism can also lead to spectral hole-burning, although this effect is seen only at low temperatures (19). The properties of the permanent gratings reported here are not consistent with this mechanism. The energy level scheme for Eu^{3+} in these glass hosts is not compatible with an ionization transition at the laser wavelength used in these experiments. Multiphoton transitions are not probable with the low laser powers used and not consistent with the observed power dependence of the signal intensities.

Also, no effects of refractive index changes are observed with a single laser beam as they are for photorefractive materials. In addition, the fact that optical erasure occurs only when Eu^{3+} ions are resonantly excited is not consistent with the photoionization process. No spectral evidence of Eu^{2+} was observed. Finally, the intensities of the two write beams were monitored as a function of time and no energy transfer between the two beams was observed. These two-beam mixing results show that the laser-induced grating is in phase with the laser interference pattern. This shows that the mechanism causing the grating is localized, which is not always true for gratings involving the migration of charge carriers.

Another mechanism which can produce a permanent grating is the radiation pressure exerted by an electric gradient field on an electric dipole. The force due to the radiation pressure is

$$\vec{F} = (\vec{P}\cdot\vec{\nabla})\vec{E} = (\alpha/2)\vec{\nabla}|E^2| \qquad (4\text{-}3)$$

where $\vec{P}$ is the atomic dielectric dipole and α is the atomic polarizability. The atomic polarizability is given by

$$\alpha = -\lambda_o^3 \Delta\gamma_n (\gamma - \gamma_o)/32\pi^3 [(\gamma - \gamma_o) + \Delta\gamma_n^2/4](1+p) \qquad (4\text{-}4)$$

where $\Delta\gamma_n$ is the natural linewidth and was measured from the absorption spectra to be approximately 30 $\mathring{A}$ and p is the saturation parameter which for this case is negligible. For excitation with λ = 465.8 nm, $\gamma = 6.440 \times 10^{14}$ Hz and a $^5D_2 - {}^7F_o$ transition wavelength of λ_o = 464 nm, $\gamma_o = 6.465 \times 10^{14}$ Hz, $\Delta\gamma_n$ can also be found, $\Delta\gamma_n = c\Delta\lambda/\lambda^2 = 4.2 \times 10^{12}$ Hz. The atomic polarizabiltiy was found from Equation 4-4 to be $9.92 \times 10^{-23} m^3$.

The square of the electric field inside the sample is

$$E^2 = E_o^2 \cos (2\pi r/\Lambda) \tag{4-5}$$

where Λ is the grating wavelength and was calculated to be 2.5×10^{-4}cm for a write beam crossing angle of approximately 10^{o}. Thus the gradient of the squared electric field is

$$\nabla|E^2| = -2\pi E_o^2[\sin (2\pi r/\Lambda)]/\Lambda \tag{4-6}$$

which has a maximum value of 8.38×10^{-2} statvolt^2/cm^2.

Finally, the force exerted by the gradient of the electromagnetic field on the electric dipole can be calculated using Equation 4-3. This force was calculated to be 1.05×10^{-13} dynes which is much too small to be considered as the source of the permanent structural modification seen in the samples.

Thermal processes can also produce refractive index changes. Laser-induced stress-optic changes including some permanent effects have been seen in rare earth-doped glasses (20). However, these observations were not dependent on having crossed laser beams and took place at higher powers than those used in these experiments. If local heating effects are the origin of the observed permanent grating, they sould be described by the thermal conductivity equation,

$$\partial Q/\partial t = -\kappa A \nabla T \tag{4-7}$$

where $\partial Q/\partial t$ is the heat deposited by the laser in an area A, κ is the thermal conductivity of the glass, and ∇T is the local temperature gradient produced by this heat. The power absorbed by the sample when irradiated by approximately 100 mW was .125 mW. The heat absorbed by the

sample will not be exactly equal to this due to radiative processes. However, this will give an upper limit to the heat created. For the glasses used in this work, the thermal conductivities are typically of the order of 10^{-2} cm^{-1} K^{-1} and a beam cross sectional area of less than 0.02 cm. The temperature gradient can be expressed as $\nabla T = \Delta T/(\Lambda/2)$ with ΔT the temperature difference between the peak and valley regions of the gratings. Λ is the grating spacing. Thus the temperature difference becomes

$$\Delta T = \dot{Q}\Lambda/2\kappa A. \qquad (4\text{-}3)$$

Using the above conditions, the local rise in temperature is approximately 3.13×10^{-4}K. In addition, these numbers over estimate ΔT because all of the laser power absorbed by the Eu^{3+} is not converted to heat. Thus, standard local heating effects are not large enough to produce any permanent modifications of the glass.

The analysis given in the previous paragraph assumes a thermalized "phonon" bath in the host material. This condition is not satisfied in the local regions where the laser power is absorbed. The radiationless relaxation transitions of rare earth ions in glasses have been shown to be "multiphonon" emission processes (21), each of which generates several high energy "phonons", of the order of 1000 cm^{-1}. Since these are generated by the Eu^{3+} ions and the thermal diffusion in the glass host is slow, the phonons are localized thus creating a high level of nonthermalized vibrational energy around each ion. This can produce a local "effective temperature" which is extremely high compared to the thermal equilibrium temperature reached when these high energy "phonons" migrate away from their origin and become thermalized with the "phonon" modes of

the host. For the radiationless relaxation processes of the Eu^{3+} ions under the excitation conditions of this experiment, local "effective temperatures" of the order of several thousand Kelvin can be produced. This is easily enough to allow ionic motion over short ranges and thus produce a local structural modification of the host glass.

Based on the above discussion, we propose a model for the laser-induced permanent grating described by the configuration coordinate diagram shown in Figure 15. It is assumed that the network forming and modifier ions of the glass host can arrange themselves in two possible configurations in the local environment of the Eu^{3+} ions, leading to double minima potential wells for the Eu^{3+} energy levels. For simplicity, only the three terms of the Eu^{3+} ions of direct relevance to the optical transitions of interest here, are shown in Figure 15. The material is assumed to have a different index of refraction depending on which configuration is present. Under normal conditions of optical excitation and decay, the configuration coordinates appear as the solid lines in Figure 15, and the ions will remain in the lower energy configuration, designated as I. The generation of local thermal energy may allow some of the ions to cross the potential barrier into configuration II, but it also will cause transitions in the reverse direction. The relative occupations of the two potential configuration will remain in thermal equilibrium, and as the local temperature returns to normal there will be a predominant occupancy of the lower energy potential well. However, with crossed laser beams, there is a gradient in the number density of high energy "phonons" resulting in a gradient in the local "effective temperature." On a microscopic scale, the atomic motion involved in the

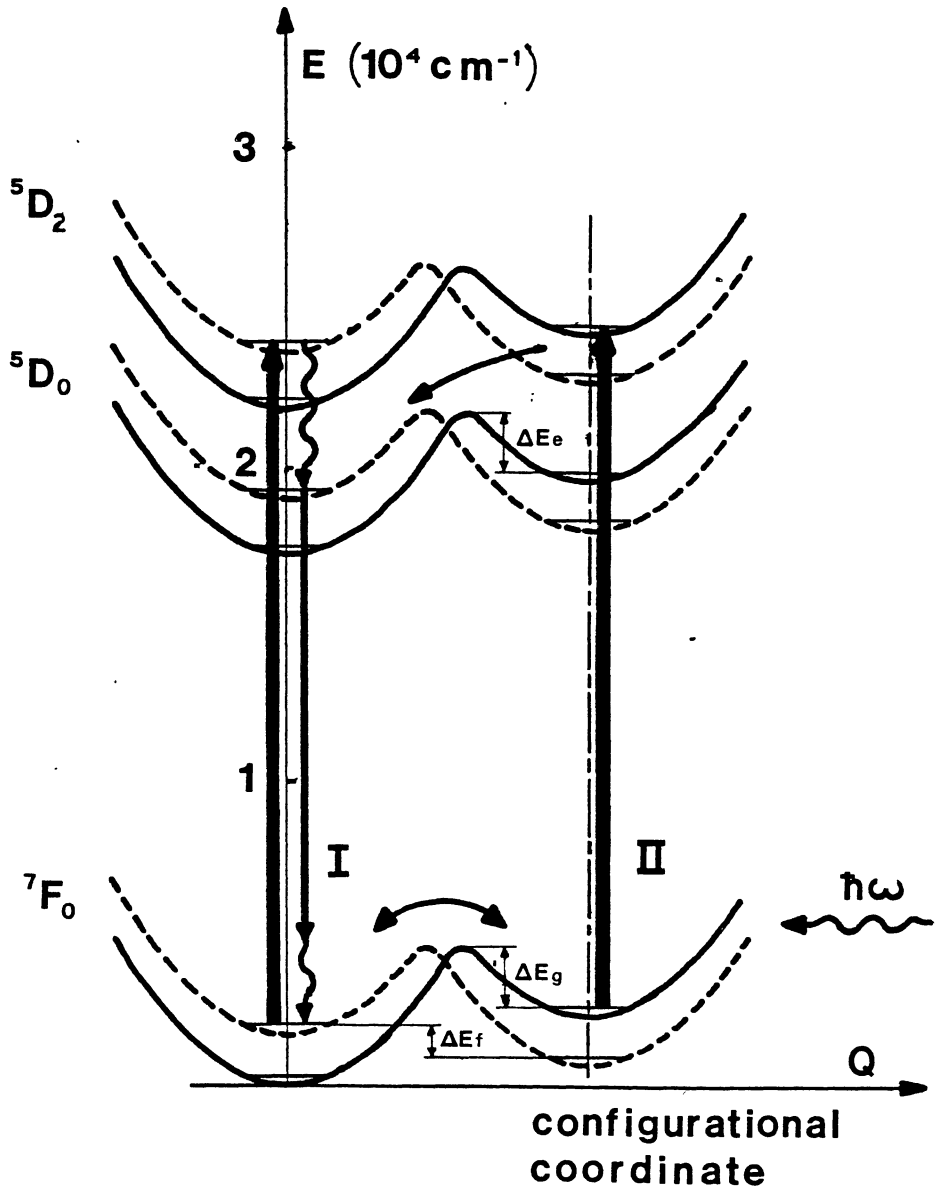

Figure 15. Configuration Coordinate Model for Laser-Induced Permanent Gratings in Eu^{3+}-Doped Glass. The Diagram Shows the Relevant Energy Levels of the Eu^{3+} Ions with Two Possible Local Configurations of the Glass, I and II. The Solid Curves are for Normal Conditions of Excitation and Decay. The Broken Curves Represent the Change in Potential Coordinates Due to the Presence of Crossed Laser Beams which Creates a Directional Bias for Ion Motion. (See Text for Explanation of Transitions Shown in the Model.)

configurational rearrangement can be described as an ionic conduction process involving only a few steps. In this picture the tendency of the vibrating atoms is to diffuse away from the peak of the temperature gradient. This gives a directional bias to the hopping of the atoms between sites of the different configurations. The resulting bias can be schematically represented by the change from the solid to the broken line potential curves in Figure 15. This shifts lower potential minimum from configuration I to configuration II and thus builds up an increased population in configuration II. Even if this effect is quite small, over the several minute time period of the grating buildup a significant change in configuration occupancy can be produced. When the crossed laser beams are turned off, the directional bias is removed and the configuration coordinates shift back to those shown by solid lines in Figure 15, but the population built up in II remains. Since this "frozen in" distribution of excess occupation of II has the shape of the laser interference pattern, it appears to the probe beam as a refractive index grating.

The transitions shown in Figure 15 represent the processes involved in the formation and erasure of the permanent grating. Initially the ions predominantly occupy configuration I in the solid line coordinate representation. During the grating formation period, crossed laser beams are tuned to resonance with the $^7F_0$ - $^5D_2$ transition of the Eu^{3+} ions. This produces the directional bias to shift the coordinate curves to the broken lines, as discussed above, and excites some of the Eu^{3+} ions to the $^5D_2$ level. The excitation energy is dissipated partially by radiative transitions to the ground terms and partially by radiationless transitions to the $^5D_0$ level through the emission of several high energy phonons. The $^5D_0$ level also has radiative transitions to the ground terms. Most

of the fluorescence transitions from both multiplets of the ^5D term terminate on the upper multiplets (J=1-6) of the ^7F term and then decay through radiationless transitions to the $^7F_0$ ground state multiplet. These processes generate several more high energy phonons. The phonons produced through both excited state and ground state radiationless transitions provide the thermal energy needed to increase the occupancy of configuration II.

From this model, the refractive index can be written as the sum of the contributions from both configurations,

$$n = N_I n_I + N_{II} n_{II} \tag{4-9}$$

where N_I and N_{II} are the populations of the two potential wells and n_I and n_{II} are the indices of refraction for the two configurations. For thermal equilibrium with the laser write beams on

$$N_I/N_{II} = \exp(\Delta E_f/kT) \tag{4-10}$$

where ΔE_f is the energy difference between the potential minima for the two configurations in the presence of the crossed laser beams and k is Boltzmann's constant. The FWM signal is proportional to the square of the difference of the index of refraction in the peak and valley region of the grating. If the valley regions of the grating are assumed to be all in configuration I, the FWM signal is given by

$$I \propto |\Delta n_{p-v}|^2 = N_{Ip}^2 |\Delta n_{II-I}|^2 \exp[2\Delta E_f/(kT)]. \tag{4-11}$$

The p and v subscripts refer to the peak and valley regions of the grating, respectively. This shows that the measured activation energy for

the formation of the permanent grating $\Delta E_f'$ is twice the difference in the energy of the potential minima.

Erasure occurs thermally when the temperature is raised high enough to provide the energy ΔE_g needed to cross the ground state potential barrier between configuration II and configuration I. With no crossed laser beams present, the solid coordinate curve is the relevant one in Figure 15. This thermal energy allows the populations of the two potential configuration to redistribute themselves to the normal equilibrium case with predominant occupancy in configuration I. Optical erasure occurs with a single laser beam tuned to resonance with the $^7F_0$-$^5D_2$ transition between the solid coordinate curves in configuration II. Relaxation back to the equilibrium population distribution can take place by several paths. Starting from the $^5D_2$ level in II, the excited Eu^{3+} ions relax back to the ground state and crossover to the I configuration can take place at any of the levels occupied during the relaxation. Increasing the temperature will enhance optical erasure by making it easier to cross over the potential barriers such as the ΔE_e shown as an example in Figure 15. Since crossover can occur with several different barriers, it is difficult to assign an exact meaning to the measured values of ΔE_{eo}. However, as for the thermal variation of the scattering, we can use a crude model to explain the thermal variation of the optical erasure rate. Assuming the excited ions relax to the $^5D_0$ state before any cross over to a different configuration occurs, the theory of Jortner, et al. (22,23) can be used. This was developed for radiationless transitions in large molecules and has been successfully used to explain the nonradiative recombination of trapped excitons in chalcogenide glasses (24). At high temperature and strong displacement of configuration minima,

the approximate expression for the radiationless transition rate becomes

$$W_{II-I} = C^2 \left[4\pi kT/(\hbar E_M)^2\right]^{\frac{1}{2}} \exp\left[-(E_M-\Delta E)^2/(4E_M kT)\right] \qquad (4\text{-}12)$$

where C is the matrix element for the transition and $(E_M-\Delta E)^2/(4E_M)$ corresponds to the energy barrier between the two potential wells. This can be simplified in our case to

$$W_{II-I} = W_o T^{\frac{1}{2}} \exp(-\Delta E_e/\kappa T). \qquad (4\text{-}13)$$

For our data the temperature dependent prefactor is negligible and Equation 4-13 is consistent with the observed results. However, the possibility of configuration crossover in the $^5D_2$ state, or between the $^5D_2$ state of II and the $^5D_0$ state of I, or in levels of the ^7F_J manifold require that we interpret ΔE_{eo} as an "effective energy barrier" for crossover and not specifically associate it with a given level.

The different properties of the FWM signal observed in the EP and LP samples can be attributed to the different concentrations of Eu^{3+} dopant. However, the difference seen in the NS glass is much harder to analyze. Phosphate glasses have lower thermal conductivities, smaller nonlinear refractive indices, and different temperature coefficients of the refractive index compared to silicate glasses. To determine the source of this difference, various glass hosts with varying amounts of rare-earth ion dopants much be investigated.

Two-level systems have been proposed previously to explain other physical properties associated with vibrational modes in glasses (25). However, the effects of having two possible configuration potentials have generally been considered only at very low temperatures. Laser-induced refractive index changes in glasses have been observed for

different types of glasses under different experimental conditions and the results attributed to bond rearrangements associated with trapped exciton effects (3-5). This mechanism is not consistent with the results observed in our experiments. The model proposed here appears to be consistent with all of the observed characteristics of the laser-induced permanent grating. However, to verify this model more experimental data obtained on different kinds of glasses is needed.

The work reported in this thesis represents the first time an interference term has been observed due to the superposition of a transient population grating and a permanent grating due to the laser-induced structural modification of the host. This demonstrates the potential usefulness of these glasses in optical applications. Producing FWM signals in glasses of this type may be applicable in optical systems involving fiber optic transmission since it should be possible to use the techniques described herein to establish phase conjugate mirrors and optical switches directly in the glass fibers. Finally, understanding the mechanism responsible for producing the laser-induced gratings should lead to a better understanding of the local structural and vibrational properties of these types of glasses.

REFERENCES

1. Bures, J., J. Lapierre, and D. Pascale, Appl. Phys. Lett., Volume 37, 1980, pp. 860.

2. Hill, K. O., Y. Fujii, D. C. Johnson, and B. S. Kawasaki, Appl. Phys. Lett., Volume 32, 1978, pp. 647; Kawaski, B. S., K. O. Hill, D. C. Johnson, and Y. Fujii, Opt. Lett., Volume 3, 1978, pp. 66.

3. Street, R. A., Solid State Commun., Volume 24, 1977, pp. 363.

4. Tanaka, K., and A. Odajima, Appl. Phys. Lett., Volume 38, 1981, pp. 481.

5. Kwon, J. H., C. H. Kwak, and S. S. Lee, Opt. Lett., Volume 10, 1985, pp. 568.

6. Kogelnik, Herwig, The Bell System Technical Journal, Volume 48, Number 9, November, 1969, pp. 2909-2947.

7. Nelson, Keith A., Roger Casalegno, R. J. Dwayne Miller, and M. D. Fayer, Journal Chemical Physics, Volume 77, Number 3, August 1, 1982, pp. 1144-1152.

8. Hill, K. O., Applied Optics, Volume 10, Number 7, July, 1971, pp. 1695-1697.

9. Gang, Xu and Richard C. Powell, Journal of Applied Physics, Volume 57, Number 4, February 15, 1985, pp. 1299.

10. Weber, M. J., D. Milam, and W. L. Smith, Opt. Eng., Volume 17, 463 (1978); M. J. Weber, C. F. Cline, W. L. Smith, D. Milam, D. Heiman, and R. W. Hellwarth, Appl. Phys. Lett., Volume 32, 1978, pp. 403.

11. Thomazeau, I., J. Etchepare, G. Grillon, and A. Migus, Opt. Lett., Volume 10, 1985, pp. 223.

12. Feinberg, J., in Optical Phase Conjugation, edited by R. A. Fisher (Academic, New York, 1983) p. 417.

13. Eichler, H. J., J. Eichler, J. Knof, and C. Noack, Phys. Stat. Sol. A, Volume 52, 1979, pp. 481.

14. Liao, P. F., L. M. Humphrey, D. M. Bloom, and S. Geschwind, Phys. Rev. B., Volume 20, 1979, pp. 4145; P. F. Liao and D. M. Bloom, Opt. Lett., Volume 3, 1978, pp. 4.

15. Salcedo, J. R., A. E. Siegman, D. D. Dlott, and M. D. Fayer, Phys. Rev. Lett., Volume 41, 1978, pp. 131.

16. Tyminski, J. K., R. C. Powell, and W. K. Zwicker, Phys. Rev. B., Volume 29, 1984, pp. 6074.

17. Ghazzawi, A. M., J. K. Tyminski, R. C. Powell, and J. C. Walling, Phys. Rev. B., Volume 30, 1982, pp. 7182.

18. Gunter, P., Phys. Reports, Volume 93, 1982, pp. 199.

19. Winnacker, A., R. M. Shelby, and R. M. Macfarlane, Opt. Lett., Volume 10, 1985, pp. 350; R. M. Macfarlane and R. M. Shelby, in Coherence and Energy Transfer in Glasses, edited by P. A. Fluery and B. Golding (Plenum, New York, 1984), pp. 189.

20. Sauer, C. L., doctoral dissertation, University of Southern California, 1980.

21. Layne, C. B., W. H. Lowdermilk, and M. J. Weber, Phys. Rev. B., Volume 16, 1977, pp. 10.

22. Freed, K. F., and J. Jortner, J. Chem. Phys., Volume 52, 1970, pp. 6272.

23. Englman, R., and J. Jortner, Mol. Phys., Volume 18, 1970, pp. 145; Englman, R., Nonradiative Decay of Ions and Molecules in Solids, (North Holland, Amsterdam, 1979).

24. Mott, N. F., E. A. Davis, and R. A. Street, Phil. Mag., Volume 32, 1975, pp. 961.

25. Anderson, P. W., B. I. Halperin, and C. M. Varma, Phil. Mag., Volume 25, 1972, pp. 1.

VITA

Edward Grady Behrens

Candidate for the Degree of

Master of Science

Thesis: LASER-INDUCED GRATINGS IN Eu^{3+}- GLASSES

Major Field: Physics

Biographical:

Personal Data: Born in Tulsa, Oklahoma, December 14, 1961, the son of Edward and Dolores Behrens. Married to Linda J. Risinger on June 1, 1985.

Education: Graduated from C. E. Donart High School, Stillwater, Oklahoma, in May, 1980; received Bachelor of Science Degree with a double major in Physics and Mathematics in May, 1984; completed requirements for the Master of Science degree at Oklahoma State University in December, 1986.

Professional Experience: Undergraduate Laboratory Instructor, Southeastern Oklahoma State University, August, 1980, to May, 1984; Undergraduate Summer Intern, Oak Ridge National Laboratory, June, 1983, to August, 1983; Graduate Lab Instructor, Oklahoma State University, August, 1984, to December, 1984; Graduate Research Assistant, Oklahoma State University, June, 1984, to present. Member of the American Physical Society and the Optical Society of America.